

Parameter Extraction Sequence for Silicon Carbide Schottky, Merged PiN Schottky, and PiN Power Diode Models

T. R. McNutt¹, A. R. Hefner², H. A. Mantooth¹, J. L. Duliere³, D. W. Berning², and R. Singh⁴

¹University of Arkansas*
BEC 3217
Fayetteville, AR 72701

³Avanti Inc.
9205 SW Gemini Dr.
Beaverton, OR 97008

²National Institute of Standards and Technology*
Semiconductor Electronics Division
Gaithersburg, MD 20899-8120

⁴CREE Research
4600 Silicon Drive
Durham, NC 27703

Abstract—A detailed parameter extraction sequence for the comprehensive silicon carbide (SiC) power diode model is presented. The extraction sequence is applicable to any SiC diode technology. It is demonstrated for a 1.5 kV, 10 A Merged PiN Schottky (MPS); 5 kV, 20 A PiN; 10 kV, 5 A PiN; and the new commercially available 600 V, 1 A and 4 A Schottky diodes.

I. INTRODUCTION

Recently, a new class of power semiconductor devices has begun to emerge that utilizes the advantages of silicon carbide (SiC). Because power rectifiers are more easily produced than three terminal power devices, they have become the first commercially available SiC power devices, as two SiC power diode products were announced in 2001. In order for circuit designers to fully utilize the advantages of this new technology, a comprehensive compact SiC power diode model was developed [1] for use in the Saber[®] circuit simulator [2]. Since the model is based on the Mantooth unified diode model, it is capable of accurately describing forward-bias, reverse-bias, forward recovery, reverse recovery, temperature dependence, and self-heating conditions [3]-[5]. The purpose of this paper is to introduce a parameter extraction sequence that will enable the new model to be used for the variety of SiC power diodes that are being introduced as evaluation prototypes and that are becoming commercially available.

Generally speaking, there are three classes of SiC power rectifiers: (a) Schottky diodes, which offer extremely high switching speed but suffer from high leakage current; (b) PiN diodes, which offer low leakage current but show reverse recovery charge during switching and have a large junction forward voltage drop due to the wide bandgap of 4H-SiC; and (c) Merged PiN Schottky (MPS) diodes, which offer Schottky-like on-state and switching characteristics, and PiN-like off-state characteristics [6]. It has been shown that a 1500 V SiC MPS diode provides superior performance over Si diodes with voltage ratings of 600 V to 1500 V [7], and

that a SiC PiN diode has superior performance compared to Si diodes with voltage ratings from 1200 V to 5000 V [8].

The comprehensive SiC power diode model is fully capable of modeling all three classes of power diodes. The model was previously shown to accurately describe the 1.5 kV, 0.45 A MPS and 5 kV, 0.25 A PiN power diodes over a wide range of application conditions in [1]. In this paper, a detailed parameter extraction sequence for the model is presented for Schottky, MPS, and PiN power diodes. Results are presented for large-area, high-current SiC diodes using the 1.5 kV, 10 A MPS; 5 kV, 20 A PiN; 10 kV, 5 A PiN; and the new commercially available 600 V, 1 A and 4 A SiC Schottky diodes.

Although a variety of other compact diode models for circuit simulation have been introduced for silicon in the past [9]-[11], the model presented in this paper is the only diode model with proven results for all three SiC power diode technologies, a detailed parameter extraction sequence (developed in this paper), and subsequent availability in the Saber circuit simulator. Furthermore, the parameter extraction sequence developed here does not require an extensive knowledge of the device fabrication, therefore allowing users the flexibility to extract parameters from a finite set of measured data.

II. COMPREHENSIVE SiC DIODE MODEL

The model presented here is capable of modeling a wide variety of technologies, while still accurately describing forward-bias, reverse-bias, forward recovery, reverse recovery, temperature dependence, and self-heating conditions. The primary interests of the work presented here are the forward-bias condition, reverse recovery condition and the temperature dependence in these regions.

To accurately describe the terminal characteristics of the power diodes, the model uses two forms of the diode equation. First, the most widely known form

* This work was supported by the National Science Foundation Grant # ECS-0115534.

* Contribution of the National Institute of Standards and Technology is not subject to copyright. This work was partially supported by the DARPA Megawatt Solid-State Elec. Program.

$$i = IS(e^{V_j/NV_T} - 1) \quad (1)$$

is used for low-level depletion region recombination i_R , low-level injection i_L , high-level injection i_H , and emitter recombination i_E currents, where IS is the saturation current, V_j is the forward diode junction voltage, N is the emission coefficient, and V_T is the thermal voltage. Each model current component has its own saturation current (ISR , ISL , ISH , and ISE) and emission coefficient (NR , NL , NH , and NE), respectively. If it is desirable to use only one of the model's injection currents, then the low-level injection current component must be used and NH is set to undefined or *undef*. In the case that both the low- and high-level injection conditions apply, the injection current equations of the form of (1) are coupled to provide better continuity and flexibility in characterization to form

$$i_0 = \frac{2i_L}{1 + \left[1 + \left(2 \frac{ISL}{ISH} \right)^{N_{eff}} e^{V_j/V_T} \right]^{1/N_{eff}}} \quad (2)$$

where

$$N_{eff} = \frac{1}{\frac{1}{NL} - \frac{1}{NH}} \quad (3)$$

In (2), i_L is the low-level injection current that takes the form of (1).

If it is desired to model the forward recovery characteristics of power diodes, then a value of $RMOD$ should be specified (i.e., setting $RMOD$ to zero turns off the forward recovery mechanism in the model). Once a nonzero value is specified, the model then incorporates a series resistance $RMOD$ that is conductivity modulated according to

$$i_{mod} = \frac{(\mu_n + \mu_p) \cdot v_m \cdot q_m}{w^2} \quad (4)$$

where v_m is the voltage across the base, q_m is the charge present in the base, w is the dynamic base width, and μ_n and μ_p are the carrier mobilities used by the model.

Reverse recovery characteristics can also be accurately modeled. The total forward injection current i_0 is used in calculating the total injected charge q_0 . The injected charge is calculated using

$$q_0 = TT \cdot i_0 \quad (5)$$

where the carrier lifetime TT is a model parameter. This physics-based representation results in stored charge due to the forward injection current, but not the depletion region recombination or emitter recombination current. The charge, q_0 , is then divided into two portions: Q_{SW0} , the portion that is removed via sweep out effects, and Q_{R0} , the portion that

recombines or diffuses out of the drift zone. To divide the charge, the model parameter $ALPH0$ is invoked as follows:

$$Q_{SW0} = ALPH0 \cdot q_0 \quad (6)$$

and

$$Q_{R0} = (1 - ALPH0) \cdot q_0 \quad (7)$$

The decay of Q_{R0} and Q_{SW0} requires a two time constant response or *double-tau model*. The model parameters TSW and TM control the nonquasi-static charge sweep out effect and the nonquasi-static diffusion effect, respectively.

TT , TSW , and TM can be varied according to the simulation temperature, T , through relationships of the form

$$TT(T) = TT(TNOM) \cdot \left(\frac{T}{TNOM} \right)^\beta \quad (8)$$

where each time constant possesses a unique β , or *BETA*, and the model parameters are defined at a nominal temperature, $TNOM$. For convenience, the model requires $TNOM$ to be input in degrees Celsius, but it should be noted that the physics-based model equations use temperatures in Kelvin ($TNOM$ is internally converted to Kelvin).

Each current component's saturation current IS is also a function of temperature. Their relationships have the following form

$$IS(T) = IS(TNOM) \cdot \left(\frac{T}{TNOM} \right)^{XTI/N} \cdot e^{[(T/TNOM)-1](EG/NV_T)} \quad (9)$$

where XTI is the saturation current temperature parameter for each current component, EG is the semiconductor bandgap at 300K, and N is the temperature dependent emission coefficient for each current component. A more rigorous, physics-based derivation can be derived from [14] which produces a similar expression for the temperature dependence of the saturation current, but both expressions rely on fitting parameters for flexibility in characterization. Therefore (9), the most commonly used form [13], was implemented in the model. The emission coefficient of each current component has a temperature dependence given by

$$N(T) = N(TNOM) \cdot [1 + TN1(T - TNOM) + TN2(T - TNOM)^2] \quad (10)$$

where $TN1$ and $TN2$ are the linear and quadratic temperature coefficients for each current component.

The temperature dependence of the forward series contact resistance RS was implemented to provide greater flexibility in describing the series resistance due to the device and package effects. It is given by

$$RS(T) = RS(TNOM) \cdot [(T/TNOM)^\gamma + TRS1(T - TNOM) + TRS2(T - TNOM)^2] \quad (11)$$

where γ , or *GAMMA*, is the exponential temperature parameter, *TRSI* is the linear temperature parameter, and *TRS2* is the quadratic temperature parameter.

In order to properly model SiC devices over a wide range of temperatures, it is necessary to incorporate the temperature dependence of the bandgap and carrier mobilities. The temperature dependence of the bandgap is of the form

$$EG(T) = EG(300K) - 3.3 \cdot 10^{-3} \cdot (T - 300K) \quad (12)$$

and the temperature dependence of the carrier mobilities in the conductivity modulated base are of the following form:

$$\mu_n(T) = \frac{MUN}{1 + \left(\frac{N_B}{1.94 \cdot 10^{17}}\right)^{0.61}} \cdot \left(\frac{T}{300K}\right)^{-ALPHA} \quad (13)$$

and

$$\mu_p(T) = 15.9 + \frac{MUP}{1 + \left(\frac{N_B}{1.76 \cdot 10^{19}}\right)^{0.34}} \cdot \left(\frac{T}{300K}\right)^{-ALPHA} \quad (14)$$

where N_B is the doping concentration of the base and *ALPHA* is defaulted to 2.15 for SiC [12].

As can be observed from the above terminology, the model was developed with the PiN diode in mind, but due to the flexibility of the model's implementation it is also applicable to Schottky and MPS power diodes. Since both the Schottky and MPS technologies have current transport physics that are exponential in nature and their Schottky contacts induce a depletion capacitance, they can also be accurately modeled as will be demonstrated below [13], [14].

III. SiC SCHOTTKY AND MERGED PiN SCHOTTKY (MPS) DIODE MODEL EXTRACTION SEQUENCE

Table A.1 presents the methodology used to extract each model parameter. The "X" in the column for the Schottky, MPS, and PiN diode types indicates the parameters and extraction steps needed for each diode type. The shaded area in Table A.1 represents the physical and structural parameters that are calculated in the conventional manner, where the bandgap of 4H-SiC *EG* is 3.26 eV [7]; *VJ*, *CJO*, *M*, and *FC* are the usual SPICE diode junction parameters [13]; and *MUN*, *MUP*, *WB*, *NB*, and *RMOD* are used to capture the PiN forward recovery phenomenon. The unshaded area represents parameters that require extraction from measured data. The parameters are listed in the order in which they are to be extracted. The model parameters are extracted at the nominal temperature (*TNOM*), except for the temperature dependent parameters (parameters *XTIR* and below in Table A.1) that are extracted using measured characteristics over a range of temperatures, typically 25 °C to 225 °C for SiC.

The extraction techniques in this section are developed for Schottky power diodes, but are equally applicable to MPS power diodes that are operated in the junction-barrier-controlled-Schottky (JBS) mode, i.e., the inherent PiN diodes do not turn on in normal forward bias operation.

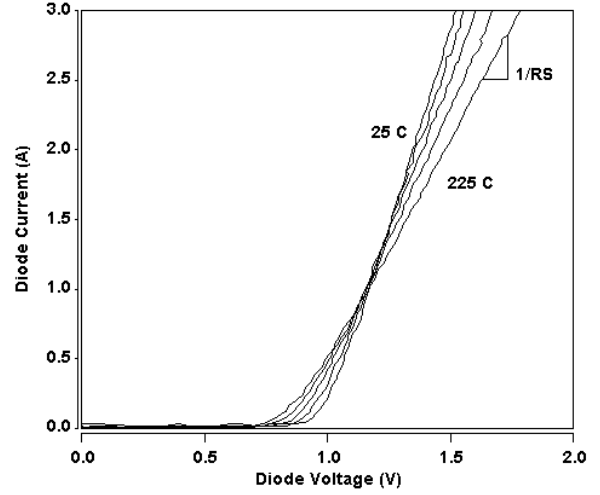


Fig. 1. Measured on-state characteristics from 25 °C to 225 °C for the 600 V, 4 A Schottky diode demonstrating the extraction of *RS* at high current densities.

The SiC diode parameter extraction sequence begins by determining the physical and structural parameters for the diode at the nominal temperature *TNOM*. As mentioned above, the parameters are named according to basic p-n junction theory, but can easily model the Schottky diode technology. In the case of the Schottky diode, the P-N grading coefficient *M* and the forward-bias depletion capacitance coefficient *FC* should be set to their default values of 0.5 [13]. The bandgap *EG* is set to the Schottky barrier voltage, which depends on the metal present (a summary of barrier heights for various metals is presented in [12]) and *VJ* is set to the built-in potential [14]. The zero-bias junction capacitance *CJO* can be calculated if enough information is available, measured from the diode's capacitance versus voltage characteristic, or it can be extracted as will be shown below.

The forward on-state characteristics are used next to extract *RS*, *ISR*, and *NR*. The on-state characteristics are modeled with a series resistance *RS* and the low-level depletion region recombination current component i_R , which has model parameters *ISR* and *NR*. Typically, for Schottky diode technologies, the emission coefficient *NR* can initially be set to 1, thus leaving only *ISR* and *RS* to be extracted versus on-state characteristics. If the model's low current region does not fit that of the measured data, then *NR* can be adjusted accordingly. The value of the forward series resistance *RS* is obtained directly from the inverse of the slope of the on-state current versus voltage characteristic at high to medium currents as shown in Fig. 1 for the 600 V, 4 A Schottky diode. After a value for *RS* is extracted, the slope of the low current portion of the on-state curve is used to extract *NR*, while the y-intercept is used to extract *ISR* using a semi-log plot. Fig. 2 shows a semi-log plot of the measured forward current versus simulated forward current in the 600 V, 4 A Schottky diode at 25 °C.

If further refinement in the low current region is desired, the model's emitter recombination current i_E can be used in

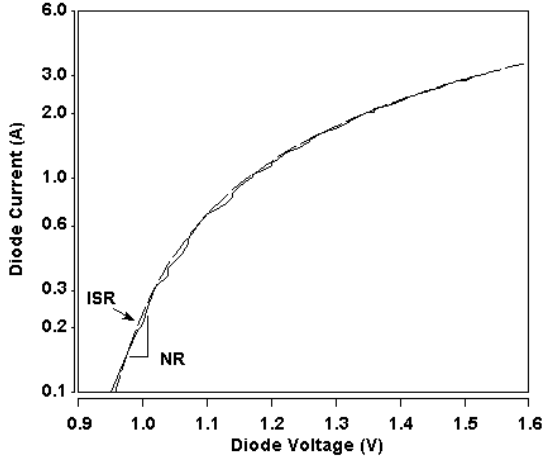


Fig. 2. Semi-log plot of the measured (solid) and simulated (dashed) forward diode current demonstrating the extraction of ISR and NR for the 600 V, 4 A Schottky diode.

combination with i_R . To do this, the low current region of the on-state characteristic curve is divided into two portions, and NE and ISE are extracted in the same manner as NR and ISR .

Once the on-state characteristics' parameters have been extracted, transient reverse recovery waveforms are used to extract the package capacitance. As previously stated, if the zero-bias value of the junction capacitance is not able to be determined either analytically or experimentally, then it can be extracted together with the package capacitance. The high-speed reverse recovery test system constructed specifically for the new SiC technology is described in [1]. The test system independently controls the turn-off forward current, reverse voltage, di/dt , dv/dt , and temperature. In the reverse recovery measurements presented here, the device is turned

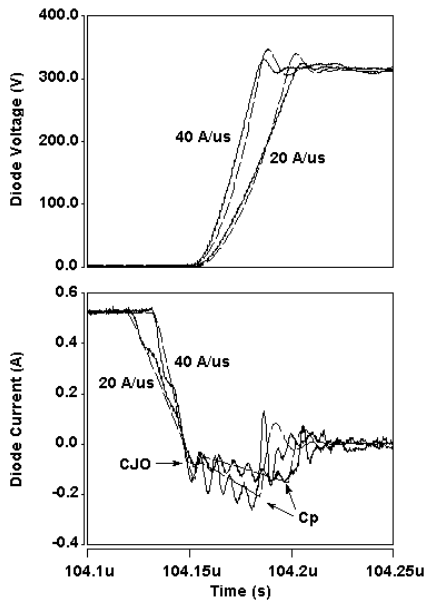


Fig. 3. Simulated (dashed) and measured (solid) reverse recovery waveforms for the 600 V, 1 A SiC Schottky diode demonstrating the extraction of CJO and the package capacitance C_p (an external library part).

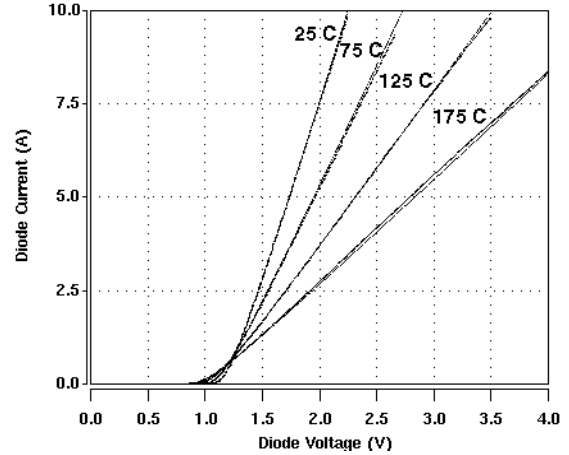


Fig. 4. Simulated (dashed) and measured (solid) on-state characteristics for the 1500 V, 10 A SiC MPS diode demonstrating the proper extraction of $XTIR$, $TRSI$, $TRS2$, and $GAMMA$.

off with a controlled di/dt . For Schottky diode technologies, the lack of stored charge reduces the reverse recovery to that of charging the depletion and package capacitances. Once the diode current crosses zero, the voltage rises as the diode depletion capacitance and package capacitance are charged. The initial reverse recovery current peak is due mainly to the junction capacitance and is accounted for by CJO , while the further increase in the negative reverse current is due to the package capacitance current, as shown in Fig. 3. At high voltages, the depletion capacitance is reduced and the package capacitance current dominates. Therefore, the package capacitance C_p is extracted from the high-voltage portion of the reverse recovery waveform. The values for C_p and CJO should be extracted such that the corresponding voltage waveforms are aligned and have the correct dv/dt .

After extracting the nominal parameters, the temperature dependent parameters are extracted. Typically, for Schottky diode technologies, majority carrier current dominates the conduction process, thus charge storage effects are negligible. In this case only the on-state characteristics temperature parameters are extracted. First, the saturation current ISR 's temperature exponent $XTIR$ is extracted using the low forward current characteristic over a range of temperatures. Next, the emission coefficient's linear $TNR1$, and quadratic $TNR2$ temperature coefficients are extracted as needed. These parameters are also extracted using the low forward current characteristics measured over a range of temperatures. The decrease in slope of the on-state characteristics (at medium to high current) as temperature increases is used to extract the parameters representing the temperature dependence of RS (i.e., a value for RS is extracted for each on-state curve versus temperature as was shown in Fig. 1). The values of RS extracted for each temperature are then used in (11) to optimize the exponential $GAMMA$, linear $TRSI$, and quadratic $TRS2$ temperature parameters for RS . Fig. 4 demonstrates the results from extracting $XTIR$, $TRSI$, $TRS2$, and $GAMMA$ for the 1.5 kV, 10 A MPS diode. Fig. 5 demonstrates the extraction of the

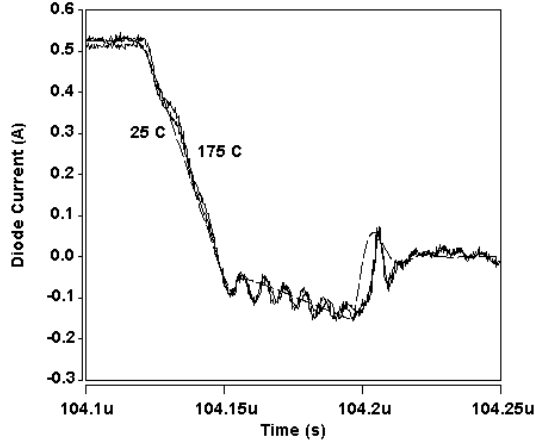


Fig. 5. Simulated (dashed) and measured (solid) reverse recovery waveforms for the 600 V, 1 A SiC Schottky diode demonstrating the extraction of the dynamic temperature parameters.

dynamic temperature parameters for the 600 V, 1 A Schottky diode (i.e., dynamic temperature parameters are set to zero).

Furthermore, if the MPS diode is biased such that the inherent PiN diodes become sufficiently forward biased, then the surge current due to the PiN diodes can also be modeled by separating the forward current due to the Schottky contacts into i_R , and the current due to the inherent PiN diodes into the injection current i_o and the emitter recombination current i_E . By properly partitioning the extraction sequence such that the Schottky/MPS sequence developed above is performed at forward bias values before turn-on of the PiN diodes, and the PiN extraction sequence developed below is performed in the high current range, emitter recombination current and charge storage effects can be easily introduced to accurately describe both the on-state and transient characteristics of the device.

IV. SiC PiN DIODE MODEL EXTRACTION SEQUENCE

In contrast to the SiC MPS diode extraction, the SiC PiN diode parameter extraction sequence requires extensive use of transient reverse recovery waveforms. The reverse recovery measurements include varying the turn-off forward current, di/dt , dv/dt , and temperature.

The SiC diode parameter extraction sequence begins by determining the physical and structural parameters for the diode. After these parameters have been calculated, the slope of the on-state curve at high to medium currents is used to extract RS . Note that if $RMOD$ is specified, then the total forward series resistance of the diode in the high current region is composed of the series combination of the contact resistance RS and the conductivity modulated drift region resistance $RMOD$. Next, the low-level injection, high-level injection, and emitter recombination current parameters are extracted. The emitter recombination parameters are the most important feature of the comprehensive SiC power diode model. For SiC, as opposed to silicon, the emitter recombination parameters should be accurately extracted to account for the low emitter efficiency that is present in these SiC devices. The emitter recombination current results in no

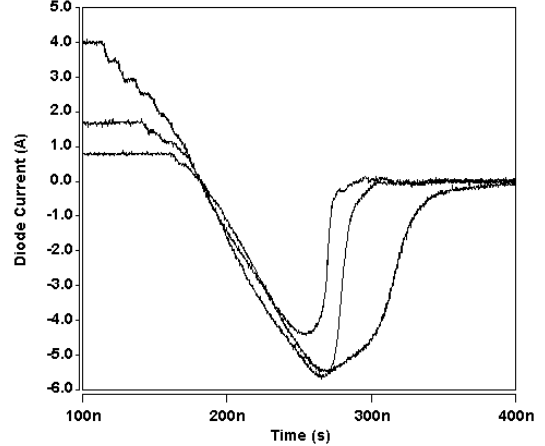


Fig. 6. Determination of emitter recombination current with reverse recovery waveforms versus forward current for the 10 kV, 5 A PiN diode. Emitter recombination dominates the conduction process after 2 A forward current.

additional reverse recovery charge, therefore it is necessary to separate out the on-state current due to forward injection and that due to emitter recombination. The low to medium current regions of the on-state curves are used to extract the low- and high-level injection currents' parameters, ISL , NL , ISH , and NH .

The remainder of the parameters are extracted using the reverse recovery waveforms. The emitter recombination current parameters (ISE and NE) are extracted from low di/dt reverse recovery waveforms as a function of forward current before turnoff. The maximum reverse current at turnoff as a function of the forward current value before turnoff is used to determine the value of forward current at which the emitter recombination current begins to dominate as shown in Fig. 6 for the case of the 10 kV, 5 A PiN diode, where the emitter recombination current dominates above 2A forward current. Fig. 7 shows the transition of total on-state current from the low- and high-level injection currents i_o to the emitter recombination current i_e for the 10 kV PiN diode. The values of ISL and ISH , and NL and NH , are extracted from the y-intercept and slope, respectively, at low to medium forward currents below the transition shown in Fig. 7, while ISE and NE are extracted at medium to high forward currents.

Once the reverse recovery current dependence has been characterized, the dynamic parameters are extracted from reverse recovery measurements for low current and low dv/dt . Extracting the dynamic parameters at low current ensures the emitter recombination current is at a minimum, and by reducing the dv/dt seen by the diode, the package and junction capacitance currents are reduced leaving only the decay of stored charge. The lifetime, TT , is extracted from the maximum reverse current and the decay of the tail current after turnoff. Once TT has been extracted, the model's two time constants are determined by separating the portion of reverse recovery current due to charge sweep out from the portion due to recombination and diffusion. The values for $ALPH0$, TSW , and TM are also extracted for low values of dv/dt . $ALPH0$ is extracted during the entire tail current decay process, while TSW is extracted during the first phase and TM

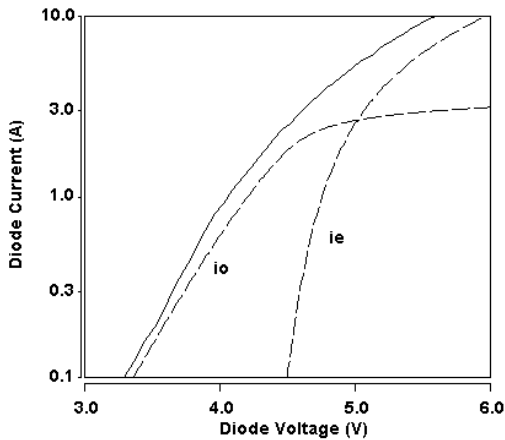


Fig. 7. Total forward current (solid) and components due to low- and high-injection i_o , and emitter recombination i_e (dashed) for the 10 kV, 5 A PiN. Emitter recombination current results in no additional reverse recovery charge.

is extracted during the second phase of the tail current decay. Fig. 8 demonstrates the extraction of the dynamic parameters TT , TSW , TM , and $ALPHO$.

The package capacitance for the PiN diode is extracted in the same manner as that of the Schottky/MPS diode using the high dv/dt reverse recovery current during the second phase. The first phase is due to stored charge recovery as described in [8]. The high-current devices characterized in this work are unpackaged, but for demonstration purposes a curve from [1] is shown in Fig. 9 demonstrating the extraction of the package capacitance and CJO for a 5 kV, 0.25 A PiN diode. Note that proper extraction of CJO and the package capacitance leads to the correct dv/dt of the voltage waveforms. Fig. 10 demonstrates the reverse recovery waveforms at two different values of di/dt for the unpackaged 5 kV, 20 A PiN diode (i.e., the package capacitance current does not dominate the second phase of the recovery current).

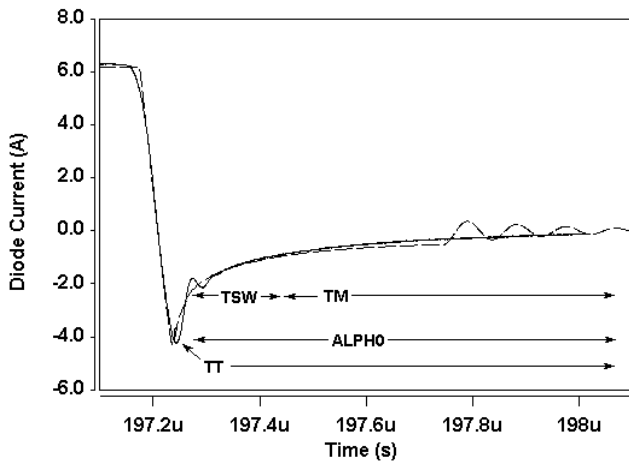


Fig. 8. Simulated (dashed) and measured (solid) reverse recovery waveforms for the 5 kV, 20 A SiC PiN diode at low dv/dt , showing the measurement used for extraction of TT , TSW , TM , and $ALPHO$.

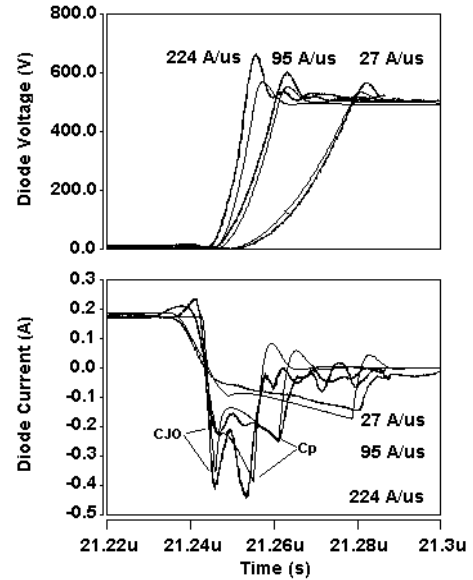


Fig. 9. Simulated (dashed) and measured (solid) reverse recovery waveforms for the 5 kV, 0.25 A PiN demonstrating the extraction of CJO and C_p .

For the PiN diode, the temperature parameter extraction is more involved than that for the Schottky/MPS. Since the PiN is a minority carrier device, the temperature dependence of the carrier lifetime and carrier sweep out effects must also be extracted in addition to the forward current parameters.

To determine the temperature characteristics of the forward diode current, measurements of the emitter recombination current, such as that shown in Fig. 6, should be performed over the temperature range. Once these measurements are complete, ISL 's and ISH 's temperature exponents, $XTIL$ and $XTIH$, are extracted at low to medium forward currents over a range of temperatures, while ISE 's temperature exponent $XTIE$ is extracted at medium to high currents. These parameters lead to curves similar to Fig. 7 for each temperature. The low-level and high-level injection

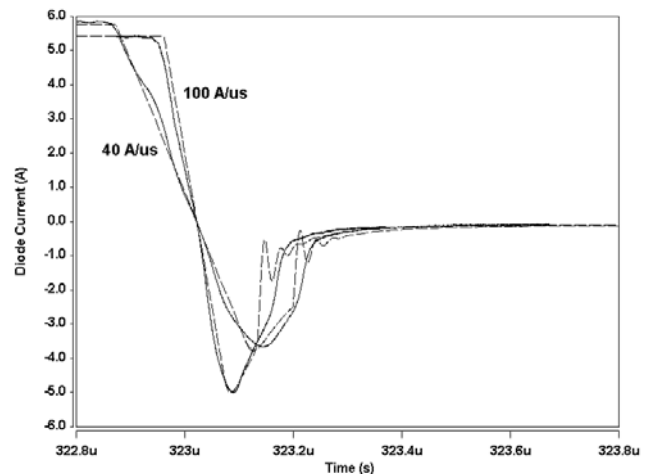


Fig. 10. Simulated (dashed) and measured (solid) reverse recovery waveforms for the unpackaged 5 kV, 20 A SiC PiN diode with switching speeds of 100 A/ μ s and 40 A/ μ s showing the results of the extraction of TT , TSW , TM , and $ALPHO$.

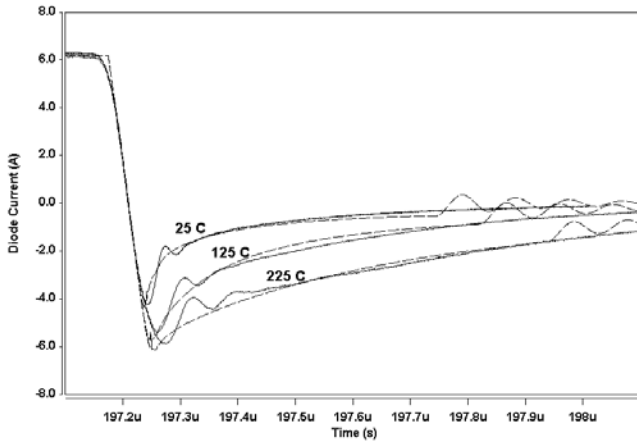


Fig. 11. Simulated (dashed) and measured (solid) reverse recovery waveforms for the 5 kV, 20 A SiC PiN diode at low dv/dt , showing the measurements used for extraction of $BETA$, $BETASW$, AND $BETAM$.

currents' emission coefficient's linear ($TNL1$, $TNHI$) and quadratic ($TNL2$, $TNH2$) temperature coefficients are also extracted at low to medium forward currents, while the emitter recombination current's linear ($TNE1$) and quadratic ($TNE2$) coefficients are again extracted at medium to high forward currents over the range of temperatures.

The PiN diode's forward series resistance, RS , has exponential ($GAMMA$), linear ($TRSI$), and quadratic ($TRS2$) temperature parameters. These parameters are extracted at medium to high currents over the measured range of temperatures. The lifetime temperature parameters ($BETA$, $BETASW$, and $BETAM$) are extracted from low dv/dt reverse recovery measurements as shown in Fig. 11, where each temperature value yields a unique TT , TSW , and TM that results in the optimization of (8). Therefore, $BETA$ is extracted from the maximum reverse current and decay of the tail current over a range of temperatures, while $BETASW$ and $BETAM$ are extracted from the first and second phases of the tail current decay over a range of temperatures.

It should be noted that the structural parameter $RMOD$ is specified only if forward recovery is desired. Specifying a value for $RMOD$ adds an iterative loop in the extraction sequence between the on-state curves at high current and the low dv/dt reverse recovery waveforms, due to the implementations of (4) and (5). An initial guess for the carrier lifetime TT is required to reduce the number of iterations.

V. CONCLUSION

A parameter extraction sequence applicable to SiC Schottky, MPS, and PiN power diodes was presented. The

sequence allows the implementation of any of the aforementioned diode technologies for a wide range of application conditions. Furthermore, the upcoming availability of the comprehensive SiC power diode model in the Saber circuit simulator along with the detailed parameter extraction sequence presented here will allow circuit designers to efficiently develop SiC component models for circuit simulation and demonstrate the advantages these devices will provide over typical silicon devices.

REFERENCES

- [1] T.R. McNutt, A.R. Hefner, H.A. Mantooth, J. Duliere, D.W. Berning, R. Singh, "Silicon Carbide PiN, Schottky, and Merged PiN-Schottky Power Diode Models Implemented in the Saber Circuit Simulator," *Conf. Proc. of IEEE Power Electronics Specialists Conference (PESC)*, pp. 2103-2108, Vancouver, Canada, June 2001.
- [2] *Saber* is a registered trademark of Avant! Inc., 9205 SW Gemini Dr., Beaverton, OR, 97008. Certain commercial products or materials have been identified in order to specify or describe the subject matter of this paper adequately. This does not imply recommendation or endorsement by the National Institute of Standards and Technology, nor does it imply that these products are the best for the purpose.
- [3] H. A. Mantooth, J. L. Duliere, "A unified diode model for circuit simulation," *IEEE Trans. on Power Electronics*, vol. 12, no. 5, September 1997.
- [4] J. L. Duliere, H. A. Mantooth, R. G. Perry, "A systematic approach to power diode characterization and model validation," *Conference Record of the Industry Applications Conference*, vol. 2, pp. 1069-1075, 1995.
- [5] H. A. Mantooth, "A unified diode model with self-heating effects," *Proceedings of the Bipolar/BiCMOS Circuits and Technology Meeting*, pp. 62-65, 1995.
- [6] R. Singh, S. Ryu, J. Palmer, A. Hefner, J. Lai, "1500 V, 4 Amp 4H-SiC JBD Diodes," *Proceedings of the 2000 International Symposium on Power Semiconductor Devices and ICs*, pp. 101-104, May 2000.
- [7] A. Hefner, D. Berning, J. Lai, C. Liu, R. Singh, "Silicon Carbide Merged PiN Schottky Diode Switching Characteristics and Evaluation for Power Supply Applications," *Conference Recordings of IEEE IAS Annual Meeting*, vol. 5, pp. 2948-2954, October 2000.
- [8] A.R. Hefner, R. Singh, J.S. Lai, D.W. Berning, S. Bouche, C. Chapuy, "SiC Power Diodes Provide Breakthrough Performance for a Wide Range of Applications," *IEEE Trans. on Power Electronics*, vol. 16 no. 2, pp. 273-280, March 2001.
- [9] P. Lauritzen, C. Ma, "A simple power diode with forward and reverse recovery," *IEEE Transactions on Power Electronics*, vol. 8, no. 4, pp. 342-345, 1993.
- [10] R. Kraus, K. Hoffman, H. Mattausch, "A precise model for the transient characteristics of power diodes," *Conf. Proc. of IEEE Power Electronics Specialists Conference (PESC)*, pp. 863-869, June 1992.
- [11] A. Yang, Y. Liu, J. Yao, "An efficient nonquasistatic diode model for circuit simulation," *IEEE Transactions on Computer-Aided Design*, vol. 13, no. 2, pp. 231-239, 1994.
- [12] W. Choyke, H. Matsunami, G. Pensl, (eds.) *SiC: a review of fundamental questions and applications to current device technology*. Akademie Verlag, Vol. II, 1997.
- [13] G. Massobrio, P. Antognetti, *Semiconductor Device Modeling with SPICE*, New York, NY: McGraw-Hill, Inc., 1993.
- [14] S. M. Sze, *Physics of Semiconductor Devices*, New York, NY: John Wiley & Sons, Inc., 1981.

APPENDIX A

TABLE A.1 PARAMETERS, CHARACTERISTICS, AND APPLICABLE DEVICES					
Parameter	Parameter Name	Extraction Characteristic	Schottky	MPS	PiN
<i>EG</i>	Bandgap	3.26 eV at 300 K	X	X	X
<i>VJ</i>	Built-in junction potential	Device specific	X	X	X
<i>CJ0</i>	Zero-bias junction capacitance	Device specific	X	X	X
<i>M</i>	P-N grading coefficient	Device specific			X
<i>FC</i>	Forward-bias depletion capacitance coefficient	Device specific			X
<i>MUN</i>	Electron mobility multiplier	947 cm ² /Vs for 4H-SiC [12] (Forward Recovery Only)			X
<i>MUP</i>	Hole mobility multiplier	108.1 cm ² /Vs for 4H-SiC [12] (Forward Recovery Only)			X
<i>WB</i>	Base width	Device specific (Forward Recovery Only)			X
<i>NB</i>	Base doping concentration	Device specific (Forward Recovery Only)			X
<i>RMOD</i>	Zero-bias value of intrinsic region resistance	Device specific (Forward Recovery Only)			X
<i>RS</i>	Forward series contact resistance	High to medium current on-state slope	X	X	X
<i>ISR</i>	Low-level recombination saturation current	Low current on-state region	X	X	
<i>NR</i>	Low-level recombination emission coefficient	Low current on-state region	X	X	
<i>ISL</i>	Low-level injection saturation current	Low current on-state region			X
<i>NL</i>	Low-level injection emission coefficient	Low current on-state region			X
<i>ISH</i>	High-level injection saturation current	Low to medium current on-state region			X
<i>NH</i>	High-level injection emission coefficient	Low to medium current on-state region			X
<i>ISE</i>	Emitter recombination saturation current	Low dv/dt reverse recovery current dependence			X
<i>NE</i>	Emitter recombination emission coefficient	Low dv/dt reverse recovery current dependence			X
<i>TT</i>	Base carrier lifetime	Low current, low dv/dt reverse recovery tail current			X
<i>ALPH0</i>	Initial value for voltage dependency of reverse recovery model	Low current, low dv/dt reverse recovery tail current			X
<i>TSW</i>	Charge sweep out time	Low current, low dv/dt reverse recovery tail current			X
<i>TM</i>	Transit time of base	Low current, low dv/dt reverse recovery tail current			X
<i>XTIR</i>	<i>ISR</i> temperature exponent	Low current on-state vs. temperature	X	X	
<i>XTIL</i>	<i>ISL</i> temperature exponent	Low current on-state vs. temperature			X
<i>XTIH</i>	<i>ISH</i> temperature exponent	Low to medium current on-state vs. temp			X
<i>XTIE</i>	<i>ISE</i> temperature exponent	Medium to high current on-state vs. temp			X
<i>TNR1</i>	Linear <i>NR</i> temperature coefficient	Low current on-state vs. temperature	X	X	
<i>TNR2</i>	Quadratic <i>NR</i> temperature coefficient	Low current on-state vs. temperature	X	X	
<i>TNL1</i>	Linear <i>NL</i> temperature coefficient	Low current on-state vs. temperature			X
<i>TNL2</i>	Quadratic <i>NL</i> temperature coefficient	Low current on-state vs. temperature			X
<i>TNH1</i>	Linear <i>NH</i> temperature coefficient	Low to medium current on-state vs. temp			X
<i>TNH2</i>	Quadratic <i>NH</i> temperature coefficient	Low to medium current on-state vs. temp			X
<i>TNE1</i>	Linear <i>NE</i> temperature coefficient	Medium to high current on-state vs. temp			X
<i>TNE2</i>	Quadratic <i>NE</i> temperature coefficient	Medium to high current on-state vs. temp			X
<i>TRS1</i>	Linear <i>RS</i> temperature coefficient	High to medium current on-state slope vs. temperature	X	X	X
<i>TRS2</i>	Quadratic <i>RS</i> temperature coefficient	High to medium current on-state slope vs. temperature	X	X	X
<i>GAMMA</i>	<i>RS</i> temperature exponent	High to medium current on-state slope vs. temperature	X	X	X
<i>BETA</i>	<i>TT</i> temperature exponent	Low current, low dv/dt reverse recovery tail current vs. temperature			X
<i>BETASW</i>	<i>TSW</i> temperature exponent	Low current, low dv/dt reverse recovery tail current vs. temperature			X
<i>BETAM</i>	<i>TM</i> temperature exponent	Low current, low dv/dt reverse recovery tail current vs. temperature			X